Performance of isotropic constitutive laws in simulating failure mechanisms in scaled RC beams

I. MARZEC, J. BOBIŃSKI

Gdansk University of Technology, Faculty of Civil and Environmental Engineering, Narutowicza 11/12, 80-233 Gdańsk, Poland, e-mails: irek@pg.edu.pl, bobin@pg.edu.pl

RESULTS OF NUMERICAL CALCULATIONS of reinforced concrete (RC) beams are presented. Based on experimental results on longitudinally reinforced specimens of different sizes and shapes are investigated. Four different continuum constitutive laws with isotropic softening are used: one defined within continuum damage mechanics, an elasto-plastic with the Rankine criterion in tension and the Drucker–Prager criterion in compression, a formulation coupling elasto-plasticity and damage mechanics and the concrete damaged plasticity (CDP) model implemented in Abaqus. In a softening regime, a non-local theory of integral format is applied to the first three constitutive laws. A fracture energy approach is utilised in CDP model. An ability to reproduce different failure mechanisms observed in experiments for each constitutive model is analysed. A comparison of force-displacement curves and crack patterns between numerical and experimental outcomes is performed.

Key words: Reinforced Concrete (RC) beams, Finite Element Method, elasto-plasticity, damage mechanics, non-local theory.

1. Introduction

IN NUMERICAL SIMULATIONS OF QUASI-BRITTLE MATERIALS like concrete the presence of cracks and shear zones has to be taken into account. These two phenomena lead to the occurrence of strain softening of the material (i.e. decrease of the strength with increasing the imposed strain) observed both in tension and compression. In tension, cracks start to nucleate as a band of diffused microcracks in the region of finite size, called fracture process zone (FPZ). In opposite to perfectly brittle materials, its size is not negligible with the respect to the size of the specimen. Upon further loading, these microcracks form a discrete macrocrack. The proper numerical description of cracks and shear zones is of major importance to obtain physically meaningful results.

Within continuum mechanics localisation zones (i.e. cracks and shear zones) can be defined with two alternative methods. In the first approach they are modelled in a smeared sense (displacement field continuity is not violated). Many different constitutive laws can be utilised: elasto-plastic ones [1–3], models defined

within continuum damage mechanics with isotropic [4, 5] or anisotropic [6, 7] description of the material degradation or formulations coupling mentioned ones [8–10]. Due to the strain softening incorporated into the definition of the material, the numerical simulations suffer from the mesh sensitivity. Classical continuum laws have to be enriched with a characteristic length, which reflects the heterogeneous mesostructure of the material. It can be done by using the Cosserat continuum [11, 12], applying the non-local theory in the integral [13, 14] or gradient [5, 15] format or by adding viscous terms in the dynamics [16]. As a second alternative description of cracks/shear zones, zero width displacement jumps can be introduced. It can be achieved by inserting interface cohesive elements [17, 18] or using strong discontinuity approach like the eXtended Finite Element Method (XFEM) [19, 20].

In simulations of reinforced concrete specimens, two additional issues should be also analysed. Firstly, the description of the interaction between concrete and steel reinforcement bars has to be defined. Several so-called slip-bond laws are available in the literature [21, 22]. Secondly, the complexity of failure mechanisms and crack patterns has to be addressed. In simulations of plain concrete structures only one failure mechanism is captured by a selected constitutive law usually (e.g. cracks only). Additionally, in plain concrete specimens only one/few independent cracks are formed usually. In RC elements several different failure mechanisms can be observed: steel yielding, concrete cracking in tension, concrete crushing in compression and shear failure modes with dominant normal diagonal crack displacements (so-called shear-tension failure mode) or with simultaneous significant normal and tangential diagonal crack displacements (so-called shear-compression failure mode). Moreover, observed crack patterns are very complex, cracks are not independent but they join/intersect. Smeared crack descriptions are much better in handling these phenomena, so they are commonly used in numerical simulations of RC specimens [23–25], while application of discrete cracks to RC elements is less popular [26].

The goal of the present paper is to offer numerical simulations of the beam response by the finite element (FE) model and to relate them to our laboratory tests on reinforced concrete beams subjected to four-point bending (with respect to strength and fracture) by taking different failure mechanisms into account. Thus, the attention is given to confirm the ability of different available in literature FE-models to realistically evaluate the RC-beam's load-bearing capacity and to capture the evolution of cracks. This issue is in particular important since there is still a lack of comprehensive research regarding to realistic modelling of complex failure modes in RC structures. Moreover, finding the crucial component of FE models driving the model performance in this field is still an open question. Four different continuum constitutive laws with isotropic softening are used: one defined within continuum damage mechanics, an elasto-plastic with

the Rankine criterion in tension and the Drucker–Prager criterion in compression, a formulation coupling elasto-plasticity and damage mechanics and concrete damaged plasticity (CDP) model implemented in Abaqus. A comparison of force-displacement curves and crack patterns between numerical and experimental outcomes is performed.

The paper is organised as follows. After a short introduction (Section 1), external laboratory tests, used to evaluate results of numerical calculations, are described in Section 2. Next, the description of all constitutive laws utilised in this study is presented. In addition, the strain localisation phenomenon is introduced and the basic information on non-local theory is given. Results of numerical calculations with a comparison with experimental outcomes is depicted in Section 4. Finally, some conclusions are gathered in Section 5.

2. Experiment

2.1. Input data

As reference data, results of the experimental tests conducted at the Gdansk University of Technology were taken [27]. The main goal of the experimental campaign was to analyse the size effect phenomenon in RC beams scaled along with the depth or the length. Four point bending tests were performed on beams with longitudinal reinforcement and without (series S1 and S2) or with (series S3 and S4) transverse reinforcement (stirrups). In this paper, only series S1 and S2 are simulated (beams without stirrups). The thickness of all specimens was kept constant and it was equal to $t = 25$ cm to eliminate the influence of hydration heat.

In the series S1 beams were scaled along with the effective height D in the proportion 1:2:4 (Fig. 1a). The effective height D was taken as 18 cm, 36 cm and 72 cm for the beam denoted as S1D18a108, S1D36a108 and S1D72a108, respectively. The span length l_{eff} was kept constant ($l_{eff} = 2700$ mm) and the distance between the support and the force point (shear zone length) was $a = 108$ cm. The shear slenderness defined as $\eta_a = a/D$ was equal to 6, 3 and 1.5 for the effective height D taken as 18 cm, 36 cm and 72 cm, respectively. For each geometry three specimens were tested.

In the series S2 the effective height was kept constant as $D = 36$ cm while the shear span length a changed in the proportion 1:2:3 (Fig. 1b). Three geometries were defined with the shear span a equal to 36 cm, 72 cm and 108 cm for the beam denoted as S2D36a036, S2D36a072 and S2D36a108, respectively (in fact the beam S2D36a108 was identical with the specimen S1D36a108). As a consequence, the effective span length changed also. In this series only two specimens for each geometry were tested.
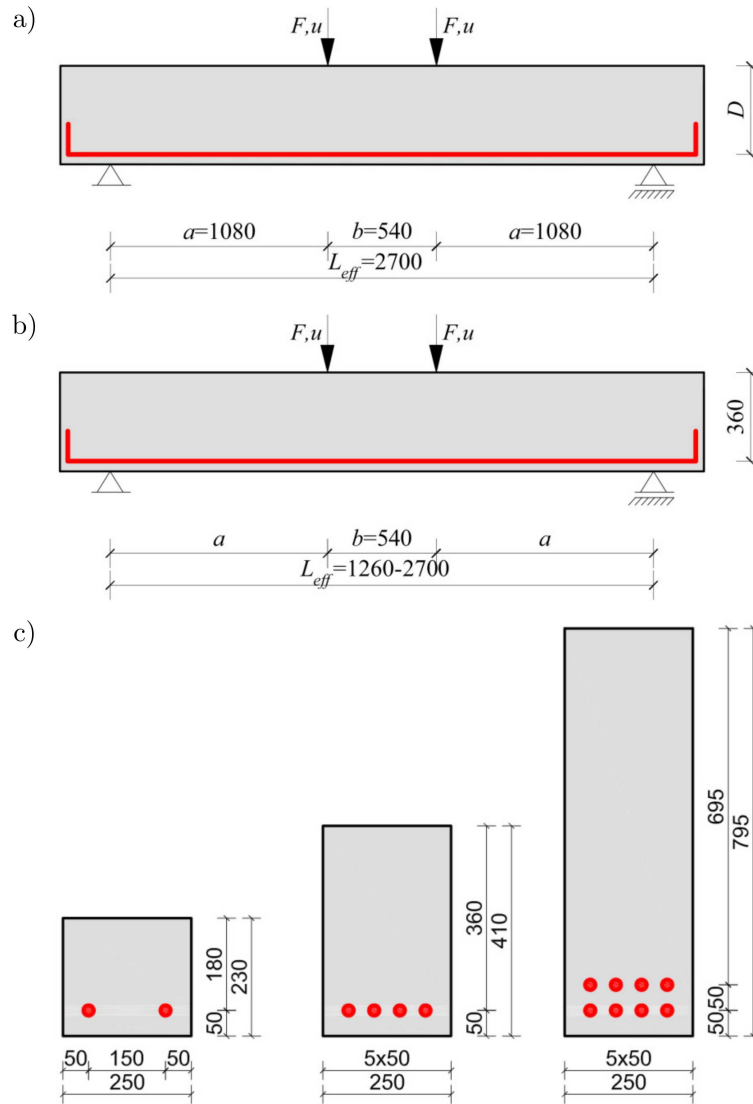
Fig. 1. Geometry and boundary conditions for the series S1 (a), series S2 (b) and cross sections with reinforcement information (c).

The reinforcement ratio was the same for all geometries, $\varrho_l = 1.4\%$. Ribbed bars of diameter 20 mm were used. The number of bars depended on the effective depth D. Two bars were placed in the beam S1D18a108, four bars – in the beams S1D36a108, S2D36a72 and S2D36a72, and eight bars (in two rows) in the beam S1D72a108. Details of the reinforcement arrangement can be seen in Fig. 1c.

2.2. Results

Several different failure mechanisms were observed in the experiments. The beam S1D18a108 failed due to yielding of the longitudinal reinforcement. A significant deflection was observed. The beam S1D36a108 failed in the so-called diagonal shear-tension failure mode (dominant opening normal crack displacements). The brittle and sudden failure mechanism was observed. The highest beam S1D72a108 collapsed due to so-called diagonal shear-compression failure (significant both tangential and normal crack displacements). Again brittle and sudden failure mechanism was observed. The beam S2D36a36 was destroyed by combined shear and compression. Two failure mechanisms were observed for the geometry S2D36a72: the diagonal shear-tension failure mode in the first specimen and diagonal shear-compression failure in the second specimen. Figure 2 presents the obtained crack patterns for all geometries. In the series S1 the nominal shear strength τ_c (calculated as $V_{\max}/tD$, $V_{\max}$ – maximum reaction force)
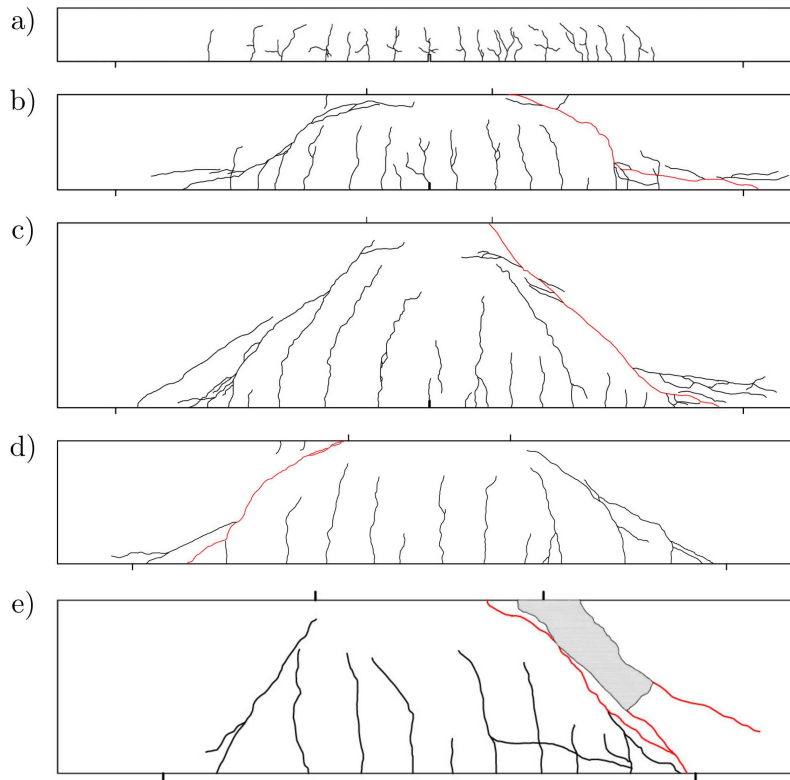

Fig. 2. Experimental crack patterns for the beam S1D18a108 (a), beam S1D36a108 (b), beam S1D72a108 (c), beam S2D36a72 (d) and beam S2D36a36 (e) (red colour – critical diagonal cracks; beams are not proportionally scaled).

increased with increasing the effective height D but it decreased with increasing the span ratio η_a. In the series S2 the nominal shear strength τ_c decreased with the increasing the span length a.

3. Constitutive laws

3.1. Isotropic damage mechanics

The first constitutive law is defined within continuum damage mechanics. A formulation proposed by Pereira *et al.* [28, 29] with some small modifications is used here. Between stresses $\boldsymbol{\sigma}$ and strains $\boldsymbol{\varepsilon}$ the following relationship is postulated:

$$(3.1) \qquad \boldsymbol{\sigma} = (1 - D)\boldsymbol{D}^e\boldsymbol{\varepsilon}$$

where $\boldsymbol{D}^e$ is the elasticity matrix and D stands for a degradation parameter. The parameter D is calculated as:

$$(3.2) \qquad D = 1 - (1 - D_t)(1 - D_c)$$

with parameters D_t and D_c to evaluate degradation in tension and compression, respectively. They depend on state variables κ_t and κ_c defined at time t as:

$$(3.3) \qquad \kappa_t(t) = \max\{\kappa_t(\tau), r^\alpha \tilde{\varepsilon}_t\}, \qquad \kappa_c(t) = \max\{\kappa_c(\tau), (1 - r)^\alpha \tilde{\varepsilon}_c\}$$

where α is a coefficient (default value $\alpha = 0.1$) and r is a triaxiality factor [30]:

$$(3.4) \qquad r(\boldsymbol{\sigma}) = \frac{\sum \langle \sigma_i \rangle}{\sum |\sigma_i|}$$

(symbol $\langle \sigma_i \rangle$ stands for a positive value of a principal stress σ_i and symbol $|\sigma_i|$ denotes an absolute value of a principal stress σ_i). Equivalent strain measures $\tilde{\varepsilon}_t$ (in tension) and $\tilde{\varepsilon}_c$ (in compression) are defined as (after [31, 32]):

$$(3.5) \qquad \tilde{\varepsilon}_t = \frac{1}{2}\frac{I_1^\varepsilon}{1 - 2v} + \frac{1}{2}\frac{\sqrt{3J_2^\varepsilon}}{1 + v}, \qquad \tilde{\varepsilon}_c = \frac{1}{5}\frac{I_1^\varepsilon}{1 - 2v} + \frac{6}{5}\frac{\sqrt{3J_2^\varepsilon}}{1 + v},$$

where I_1^ε and J_2^ε are the first invariant of the strain tensor and the second invariant of the deviatoric strain tensor, respectively, and v denotes Poisson's ratio. The evolution of the degradation parameter D_t (D_c) is described with an exponential formula ($i = t, c$):

$$(3.6) \qquad D_i = 1 - \frac{\kappa_{i0}}{\kappa_i}\Big(1 - \alpha_i + \alpha_i \exp(-\beta_i(\kappa_i - \kappa_{i0}))\Big)$$

with parameters κ_{i0}, α_i and β_i (two sets in total). This is the only deviation from the original model (a much more complex relationship was used in [28, 29]).

3.2. Elasto-plasticity

The second constitutive law is defined within elasto-plasticity. In tension the Rankine criterion with isotropic softening defines yielding of the material:

$$(3.7) \qquad f_t = \max\{\sigma_1, \sigma_2, \sigma_3\} - \sigma_t(\kappa_t)$$

where σ_i – the principal stress, $\sigma_t(\kappa_t)$ – the tensile yield stress and κ_t – the hardening/softening parameter equal to the maximum principal plastic strain ε_1^p. The associated flow rule is assumed. The tensile yield stress can be defined as a linear function, bilinear relationship [33], standard exponential formula or as an exponential function proposed by HORDIJK [34].

In compression the linear Drucker–Prager criterion with isotropic hardening and softening is used with the following yield function:

$$(3.8) \qquad f_c = q + p \cdot \tan \varphi - \left(1 - \frac{1}{3} \cdot \tan \varphi\right)\sigma_c(\kappa_c),$$

where q – the Mises equivalent deviatoric stress, p – the mean stress, φ – the internal friction angle, $\sigma_c(\kappa_c)$ – the compression yield stress (tabular data), κ_c – the hardening/softening parameter equal to the maximum plastic vertical normal strain during uniaxial compression $|\varepsilon_{11}^p|$. The flow potential is defined as:

$$(3.9) \qquad g_c = q + p \tan \psi$$

with the dilatancy angle ψ. Invariants q and p are defined as (s_{ij} is a deviatoric stress tensor):

$$(3.10) \qquad q = \sqrt{\frac{3}{2}s_{ij}s_{ij}} \quad \text{and} \quad p = \frac{1}{3}\sigma_{kk}.$$

More information about the formulation can be found in [35, 36].

3.3. Coupled formulation

The next constitutive law couples continuum damage mechanics with elasto-plasticity [37–39]. The idea follows the proposal by PAMIN and DE BORST [8]. It is based on the strain equivalence hypothesis. Elasto-plasticity is defined in effective stress space. Rankine and Drucker–Prager criteria described in Section 3.1 are utilised. The only difference is the definition of the yield functions σ_t and σ_c. A linear hardening with the modulus equal to $E/2$ (E – Young's modulus) is assumed here for both criteria.

The softening of the material is described via isotropic damage with an equivalent strain measure $\tilde{\varepsilon}$ defined in total strains taken after MAZARS [4]:

$$(3.11) \qquad \tilde{\varepsilon} = \sqrt{\sum\langle\varepsilon_i\rangle^2}$$

where ε_i is a principal strain. The state variable κ and two additional quantities κ_t and κ_c to describe stiffness degradation in tension and softening, respectively, are defined:

$$(3.12) \qquad \kappa = \max_{\tau \le t} \tilde{\varepsilon}(\tau), \qquad \kappa_t = r\kappa, \qquad \kappa_c = (1-r)\kappa.$$

The degradation parameter D is described via the formula:

$$(3.13) \qquad D = 1 - (1 - s_c D_t)(1 - s_t D_c)$$

where s_c and s_t are splitting functions. The degradation parameter in tension D_t is defined with Eq (3.6), state variable κ_t and parameters κ_0, α and β. The degradation parameter in compression is calculated using the relationship (after [40]):

$$(3.14) \qquad D_c = 1 - \left(1 - \frac{\kappa_0}{\kappa_c}\right)\left(0.01\frac{\kappa_0}{\kappa_c}\right)^{\eta_1} - \left(\frac{\kappa_0}{\kappa_c}\right)^{\eta_2} \exp(-\delta_c(\kappa_c - \kappa_0))$$

with parameters η_1, η_2 and δ_c. Note that the same value of κ_0 is used to calculate both degradation parameters D_t and D_c. Full description and more details of the performance of the model can be found in [39].

3.4. Concrete damaged plasticity

As the last alternative, a constitutive law implemented in commercial program Abaqus [41] was chosen. It is based on the model proposed by Lubliner *et al.* [42] and later improved by Lee and Fenves [30]. A single yield envelope is defined within effective stresses. Two hardening/softening parameters govern the softening and/or hardening of the material in tension and compression. A noncircular shape of the yield function on the deviatoric plane can be obtained by taking the parameter K smaller than one. A hyperbolic Drucker-Prager function defines the flow potential with an eccentricity ϵ. In addition, damage degradation can be activated independently of tension and compression yielding. The detailed description of the model (with equations) can be found in [41].

3.5. Regularisation

Numerical simulations with classical continuum constitutive laws with softening do not produce reliable results. Obtained outcomes are mesh dependent because the boundary value problem is ill-posed. In order to restore the well-posedness of the boundary value problem information about a characteristic length of the microstructure has to be added. One of the possibilities comes

with the integral non-local theory. It replaces a local value of the variable controlling the softening of the material by its non-local counterpart, calculated as an averaged quantity over neighbours.

In calculations with the isotropic damage constitutive law (Section 3.1) equivalent strain measures are averaged according to the formula:

$$(3.15) \qquad \bar{\varepsilon}(\boldsymbol{x}) = \frac{\int_V w(\|\boldsymbol{x} - \boldsymbol{\xi}\|)\tilde{\varepsilon}(\boldsymbol{\xi})d\boldsymbol{\xi}}{\int_V w(\|\boldsymbol{x} - \boldsymbol{\xi}\|)d\boldsymbol{\xi}}$$

where $\boldsymbol{x}$ – a considered point and $\boldsymbol{\xi}$ – neighbour points. As a weighting function w the Gauss distribution function is used:

$$(3.16) \qquad w(r) = \frac{1}{l_c\sqrt{\pi}} \exp\left(-\left(\frac{r}{l_c}\right)^2\right)$$

where l_c denotes the characteristic length of the microstructure. It should be noted that in practise the averaging is restricted to the small area around the considered point (the influence of neighbour points at the distance of $r = 3 \times l_c$ is only 0.01%). Equation (3.15) is applied independently to average strain measures $\tilde{\varepsilon}_t$ and $\tilde{\varepsilon}_c$.

In calculations with elasto-plastic constitutive law (Section 3.2) softening parameters in the Drucker–Prager (κ_c) and Rankine (κ_t) criteria are defined as non-local ($\bar{\kappa}_c$, $\bar{\kappa}_t$) following BRINKGREVE [43]:

$$(3.17) \qquad \bar{\kappa}_i(\boldsymbol{x}) = (1 - m)\kappa_i(\boldsymbol{x}) + m\frac{\int_V w(\|\boldsymbol{x} - \boldsymbol{\xi}\|)\kappa_i(\boldsymbol{\xi})d\boldsymbol{\xi}}{\int_V w(\|\boldsymbol{x} - \boldsymbol{\xi}\|)d\boldsymbol{\xi}}$$

where m – the additional non-locality parameter. The parameter m has to be greater than one to obtain mesh insensitive results.

In calculations with a coupled law (Section 3.3) only damage part is "made non-local" because its mechanism is responsible for material softening. The elasto-plastic part produces no softening because it includes only hardening.

In calculations with concrete damaged plasticity model (CDP) (Section 3.4) non-local theory cannot be applied. The CDP model is a built-in feature of the Abaqus program without any modifiable features. Therefore a simpler technique is used here: fracture energy regularization [44]. It means the definition of the material in the softening regime should be scaled with respect to the size of a finite element. Additionally, Abaqus allows activating viscoplastic regularization according to the Devaut-Lions approach by defining relaxation time μ. Similar regularisation technique was used in [45].

4. Results

Numerical calculations are executed in Abaqus Standard commercial code. In all numerical calculations the following elastic parameters are assumed [39]:

Young's modulus $E = 34$ GPa and Poisson's ratio $v = 0.2$. The tensile strength is taken as $f_t = 3.2$ MPa and the compressive strength is equal to $f_c = 61$ MPa. Plane strain conditions are assumed. The characteristic length in all simulations with non-local constitutive laws is set to $l_c = 5$ mm. In the calculations with an isotropic damage constitutive law by Pereira and Sluys (Section 3.1, [28, 29]) the following material parameters are assumed (Eq. (3.6)): $\kappa_{t0} = 9.5 \cdot 10^{-5}$, $\alpha_t = 0.98$ and $\beta_t = 50$ in tension and $\kappa_{c0} = 1.8 \cdot 10^{-3}$, $\alpha_c = 0.98$ and $\beta_c = 50$ in compression. In the elasto-plastic constitutive law with Drucker–Prager and Rankine criteria (Section 3.2) the non-locality parameter m is taken as 2. In the Rankine criterion an exponential softening is assumed with the fracture energy $G_F = 100$ N/m. In the Drucker–Prager criterion the tabular definition with the hardening phase followed by the linear softening is declared. The friction angle is equal to $\varphi = 15°$ and the dilatancy angle is taken as $\psi = 8°$ In the elasto-plastic constitutive law coupled with damage (Section 3.3) formulated in [39] the initial stress in elasto-plasticity is set to 3.3 MPa and 60 MPa in tension and compression, respectively. The friction angle is equal to $\varphi = 14°$ and the dilatancy angle is taken as $\psi = 8°$. The following set of parameters describes the behaviour of the material in damage: $\kappa_0 = 9.5 \cdot 10^{-5}$, $\alpha = 0.95$, $\beta = 85$, $\eta_1 = 1.15$, $\eta_2 = 0.15$ and $\delta_c = 150$. The following parameters of the concrete damaged plasticity model from Abaqus (Section 3.4) are assumed. In tension a bilinear softening is defined with the fracture energy $G_F = 100$ N/m. In the compression criterion the tabular definition with the hardening phase followed by the linear softening is declared. In addition the stiffness degradation is declared in compression. The dilatation angle is taken as $\psi = 38°$ (its physical interpretation differs from the quantity used in the linear Drucker–Prager criterion, see Sections 4.2 and 4.3). The default values are taken to the remaining parameters. To facilitate simulations the viscosity is included with the relaxation time equal to $\mu = 10^{-4}$ (the total simulation time is assumed as 1.0). For all constitutive laws the parameters in softening are chosen in such a way to obtain similar values of the fracture energy in tension and the crushing energy in compression. The perfect equivalence is impossible due to different relationships assumed in the analysed models.

The FE mesh consisted of diagonally crossed three node (constant strain) triangular elements and the size of 5 mm. Reinforced bars are modelled as truss elements. Between steel bars and concrete cohesive interface elements are inserted with the slip-bond law proposed by Dörr [21]. He assumed the following relationship between shear stress τ and slip δ:

$$(4.1) \qquad \tau(\delta) = \begin{cases} f_t \left[5\left(\dfrac{\delta}{\delta_u}\right) - 4.5\left(\dfrac{\delta}{\delta_u}\right)^2 + 1.4\left(\dfrac{\delta}{\delta_u}\right)^3 \right] & 0 \le \delta < \delta_u, \\ 1.9 f_t & \delta > \delta_u, \end{cases}$$
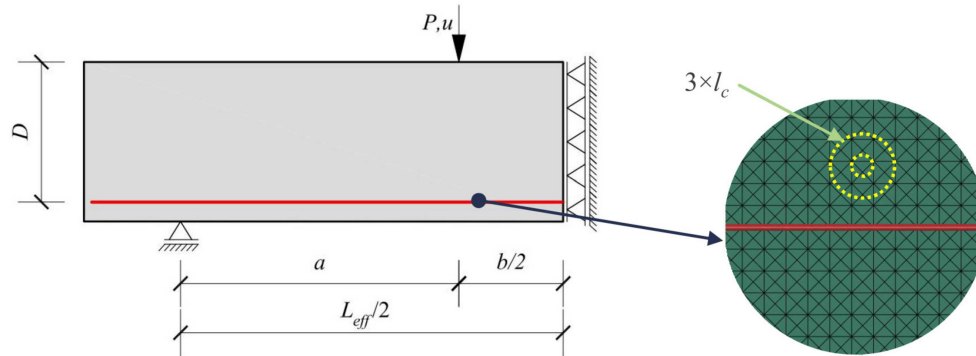
FIG. 3. Boundary conditions and FE mesh for RC beams (diameter of small yellow circle is related to characteristic length l_c and diameter of larger yellow circle is related to influence range of non-locality $3 \times l_c$).
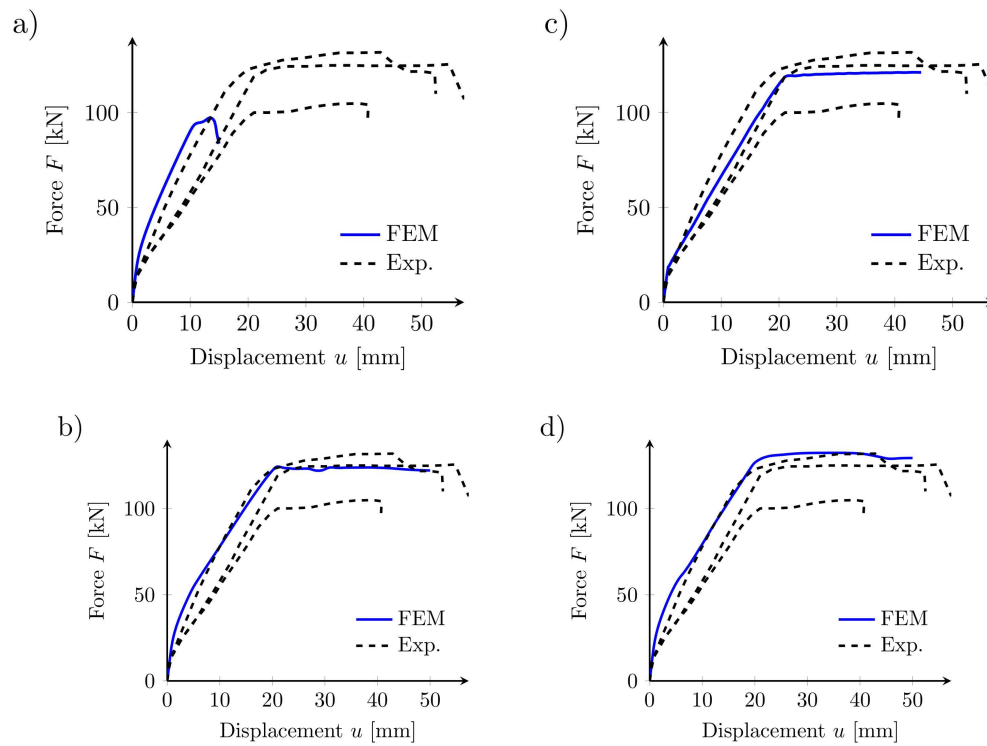

FIG. 4. Force-displacement curves obtained with the: isotropic damage model (a), elasto-plastic model (b), coupled model (c) and concrete damaged plasticity model (d) for the beam S1D18a108.

where δ_u is a critical slip equal to 0.06 mm. The assumed boundary conditions and the part of the defined FE-mesh is shown in Fig. 3.

4.1. Beam S1D18a108

First, the simulations for the specimen S1D18a108 are executed. Figure 4 presents force-displacement diagrams, while smeared crack patterns are shown in Fig. 5. The isotropic damage model is not able to capture the behaviour of the beam properly. It fails to reproduce the reinforcement yielding (no plateau on the force-displacement diagram, Fig. 4a). Due to the premature failure, the crack pattern is not developed and improper inclined cracks in the bending zone next to the axis of symmetry appear (Fig. 5a). The remaining constitutive laws reflect the experimentally observed failure mechanisms (yielding of the reinforcement, Figs. 4b–4d). Moreover, good agreement of cracks patterns is obtained (Figs. 5b–5d). Only for the concrete damaged plasticity law the crack pattern is influenced by the FE mesh definition (inclined, not vertical cracks in the bending zone next to the axis of symmetry, Fig. 5d). Moreover, much more cracks are created comparing to the simulations with other constitutive laws (the same dense FE mesh is used). This remark applies to all results with the concrete damaged plasticity model.
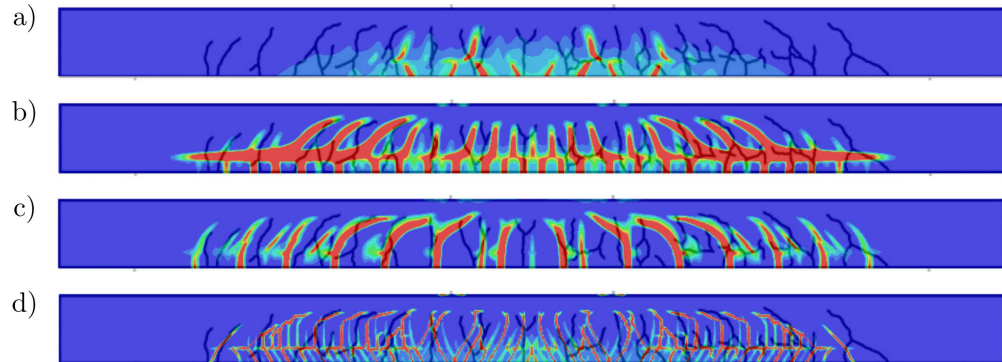

Fig. 5. Smeared crack patterns obtained with the: isotropic damage model (a), elasto-plastic model (b), coupled model (c) and concrete damaged plasticity model (d) for the beam S1D18a108.

4.2. Beam S1D36a108

The results for the specimen D1D36a108 are shown in Figs. 6 and 7 (force-displacement curves and smeared crack patterns). All constitutive laws are able to capture the failure mechanism properly (shear failure of concrete with the so-
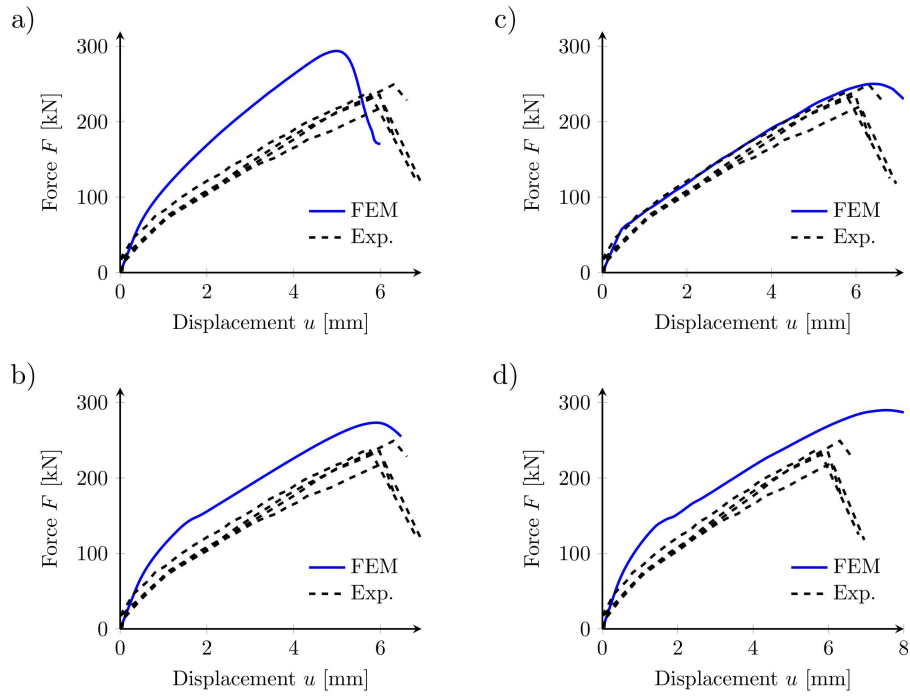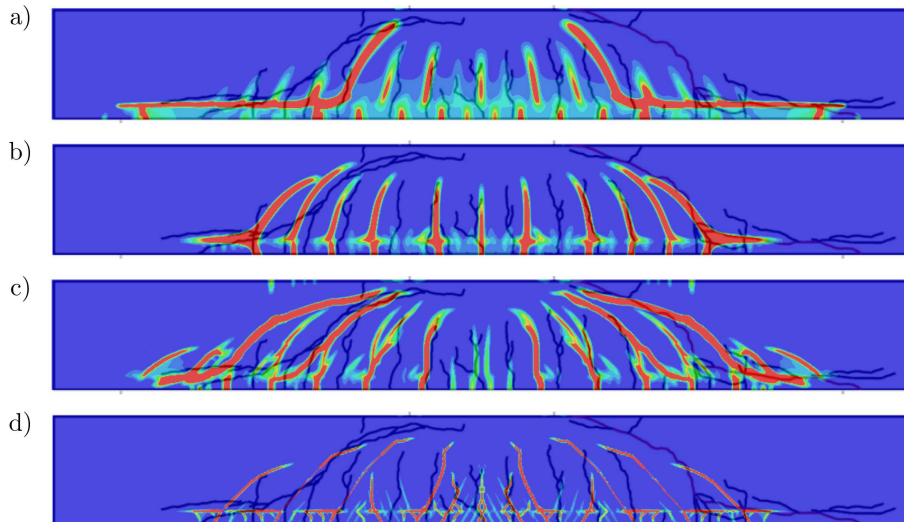
Fig. 6. Force-displacement curves obtained with the: isotropic damage model (a), elasto-plastic model (b), coupled model (c) and concrete damaged plasticity model (d) for the beam S1D36a108.

Fig. 7. Smeared crack patterns obtained with the: isotropic damage model (a), elasto-plastic model (b), coupled model (c) and concrete damaged plasticity model (d) for the beam S1D36a108.

called diagonal tension failure mode dominated), although some discrepancies
are observed (Fig. 6). The isotropic damage law overestimates and the elasto-
plasticity model slightly overestimates the peak value. The same conclusion ap-
plies to the concrete damaged plasticity law from Abaqus. Moreover, almost no
softening is present (Fig. 6d). With respect to the crack pattern, the best agree-
ment is achieved with the elasto-plasticity and coupled models (Figs. 7b and 7c).
The isotropic damage law gives generally the proper cracks map, but the criti-
cal cracks are too steep (Fig. 7a). In the concrete damaged plasticity model the
critical cracks are not fully developed (Fig. 7d).

4.3. Beam S1D72a108

Next, the simulations for the specimen S1D72a108 are performed. Figure 8
presents force-displacement diagrams, while smeared crack patterns are shown in
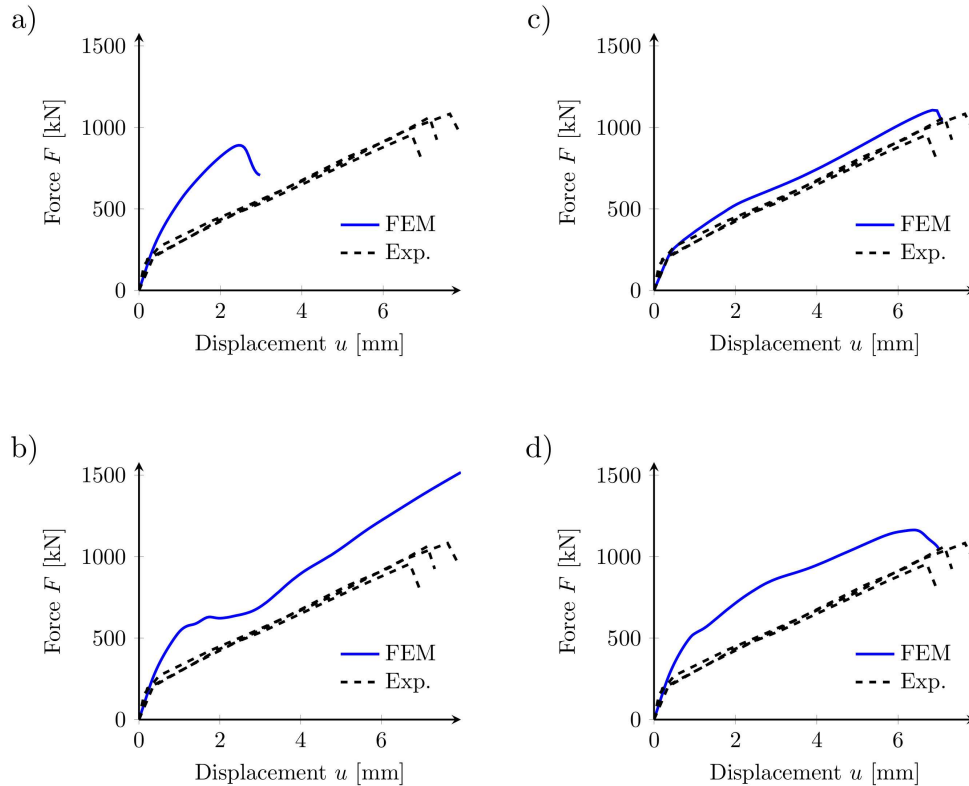Fig. 9. The maximum force obtained with the isotropic damage model (Fig. 8a)

Fig. 8. Force-displacement curves obtained with the: isotropic damage model (a),
elasto-plastic model (b), coupled model (c) and concrete damaged plasticity model (d) for the
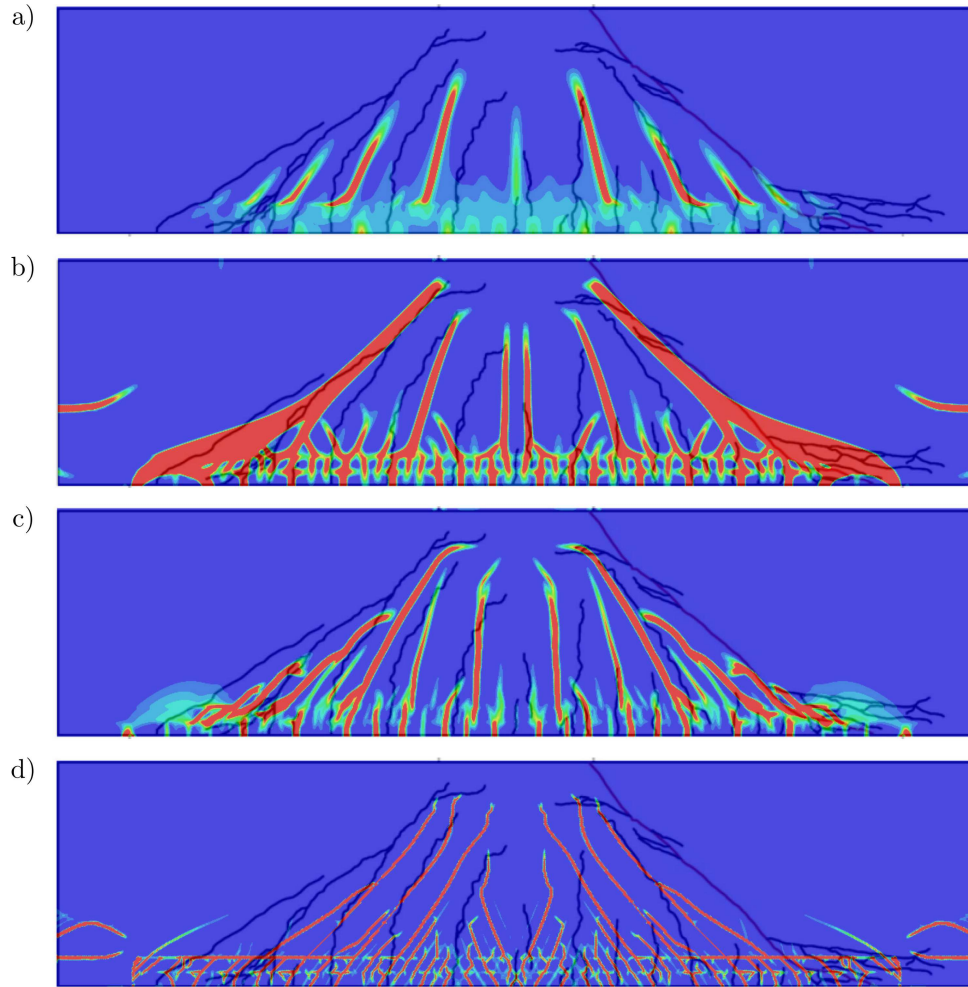beam S1D72a108.

a)

b)

c)

d)

Fig. 9. Smeared crack patterns obtained with the: isotropic damage model (a), elasto-plastic model (b), coupled model (c) and concrete damaged plasticity model (d) for the beam S1D72a108.

is close to the smaller experimental value and the softening after the peak is captured, but the curve is too stiff. There is no peak point on the force-displacement diagram obtained with the elasto-plastic law (Fig. 8b). Only the coupled model produces the force-displacement curve closed to the experimental one (Fig. 8c). The concrete damaged model gives the too stiff response and it overestimates the peak value (Fig. 8d), but the failure mechanism is properly captured. All constitutive laws are able to properly reflect the experimental crack pattern.

4.4. Beam S2D36a72

The results for the specimen D2D36a36 are shown in Figs. 10 and 11 (force-displacement curves and smeared crack patterns). Although the peak value obtained with the isotropic damage law is between experimental values (Fig. 10a), the curve is significantly too stiff. The remaining models overestimate the peak value, especially the elasto-plastic and concrete damaged plasticity ones (Figs. 10b and 10d). Moreover these two laws give too stiff force-displacement diagrams. The crack pattern for the isotropic model is not fully developed (Fig. 11a). The elasto-plastic and coupled constitutive laws give results consistent with experiment (critical cracks are clearly visible, Figs. 11b and 11c). The calculated crack pattern with the concrete damaged plasticity model can be accepted, however no dominant inclined localized zones are obtained (Fig. 11d).
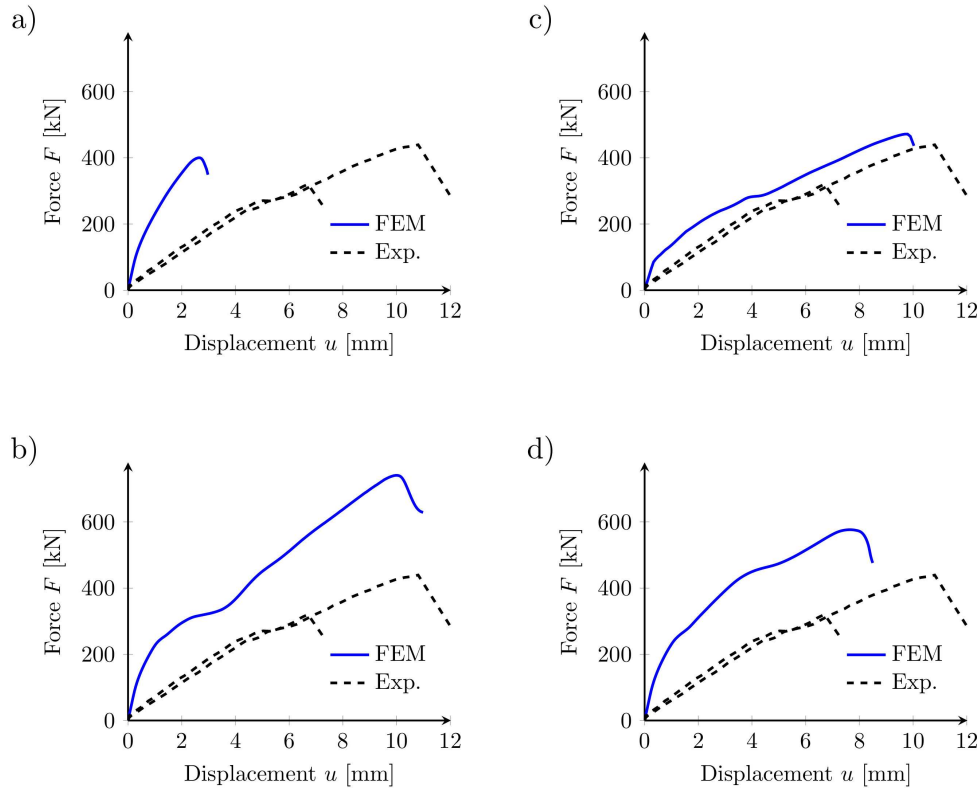

FIG. 10. Force-displacement curves obtained with the: isotropic damage model (a), elasto-plastic model (b), coupled model (c) and concrete damaged plasticity model (d) for the beam S2D36a72.
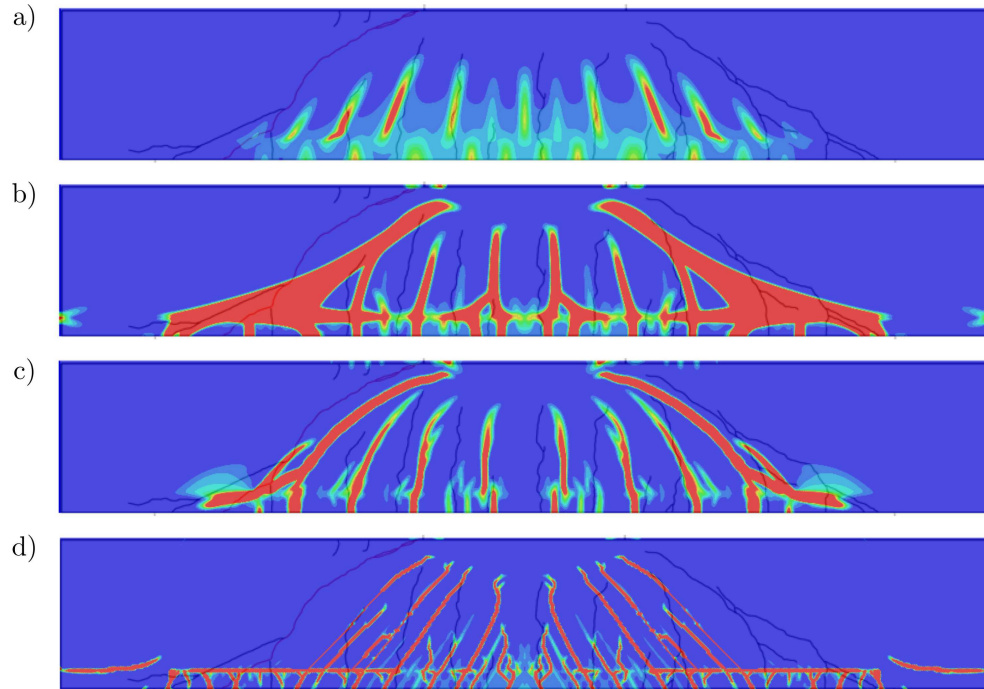
Fig. 11. Smeared crack patterns obtained with the: isotropic damage model (a), elasto-plastic model (b), coupled model (c) and concrete damaged plasticity model (d) for the beam S2D36a72.

4.5. Beam S2D36a36

Finally, simulations for the specimen S3D36a36 are performed. Figure 12 shows the force-displacement curves, while the crack patterns are depicted in Fig. 13. The isotropic model underestimates the peak law and the curve is too stiff. Also, too stiff response is obtained with the elasto-plastic law, but the peak value is between the experimental values. Both coupled and concrete damaged plasticity models return good force-displacement curves. Despite some discrepancies on the force-displacement curves, all constitutive laws produce proper crack patterns.

4.6. Other parameters

In addition, an influence of the mesh size on the results obtained with the concrete damaged model (CDP) is investigated. Except for the fine mesh (FE size 5 mm) used in above-presented calculations, a coarse mesh is also defined with the FE size equal to 1 cm. The FE size acts as a characteristic length, therefore
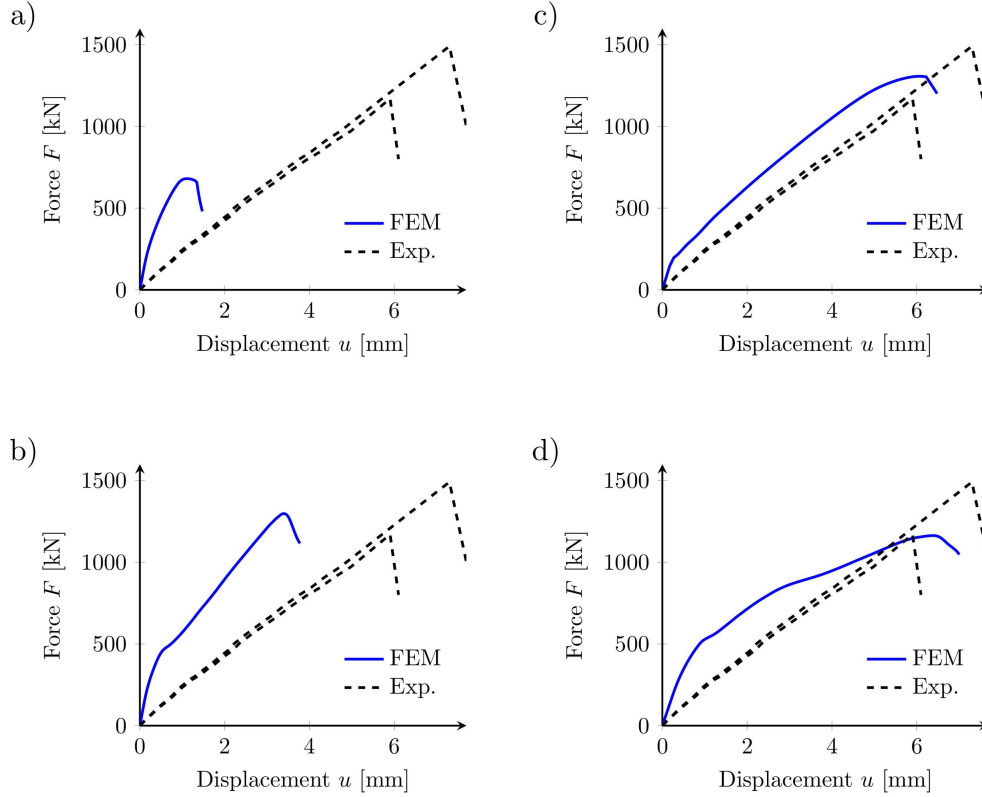
Fig. 12. Force-displacement curves obtained with the: isotropic damage model (a), elasto-plastic model (b), coupled model (c) and concrete damaged plasticity model (d) for the beam S2D36a36.

the modification of the material definition is needed for CDP model. All softening curves are scaled to keep the fracture energy in tension and the crushing energy in compression unchanged. Obtained crack patterns are shown in Fig. 14. For all specimens the same failure mechanism is obtained with both FE-meshes. The coarse FE mesh gives wider cracks, but despite some minor differences, the principal cracks are the same. The differences in maximum forces are smaller than 5% for all beams, only for the specimen S1D36a108 larger discrepancy is obtained (18%).

It should be also noted that the bond-slip law has a minor influence on the results when a realistic relationship between shear stress and relative displacement along steel bars is assumed (especially its initial stiffness). Only when the initial stiffness is unrealistically low, the smaller number of cracks is obtained [39].
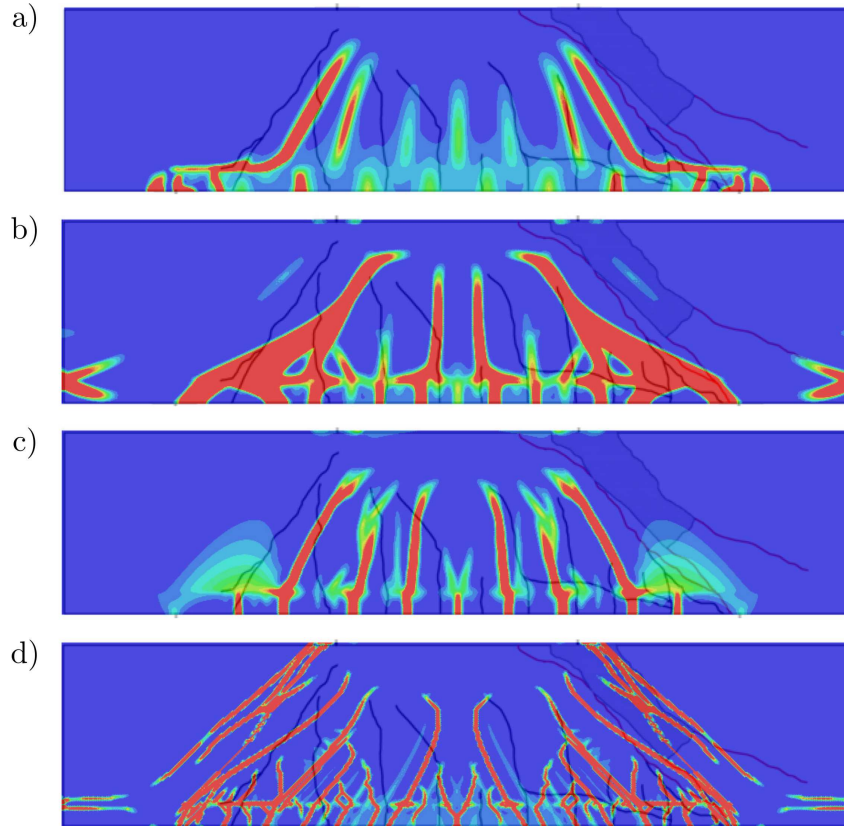
Fig. 13. Smeared crack patterns obtained with the: isotropic damage model (a), elasto-plastic model (b), coupled model (c) and concrete damaged plasticity model (d) for the beam S2D36a36.

5. Conclusions

In the paper numerical simulations of the different failure mechanisms in RC beams under four-point bending were presented. Four different constitutive laws with isotropic softening were analysed: one defined within continuum damage mechanics, an elasto-plastic with the Rankine criterion in tension and the Drucker–Prager criterion in compression, a formulation coupling elasto-plasticity and damage mechanics and the concrete damaged plasticity (CDP) model implemented in Abaqus. Comparison of global quantities: force-displacement diagrams and crack patterns was performed. Analysing the ability to properly capture the failure mechanism the best results were obtained with both: the coupled elasto-plastic model and the CDP model from Abaqus. The worst results were obtained
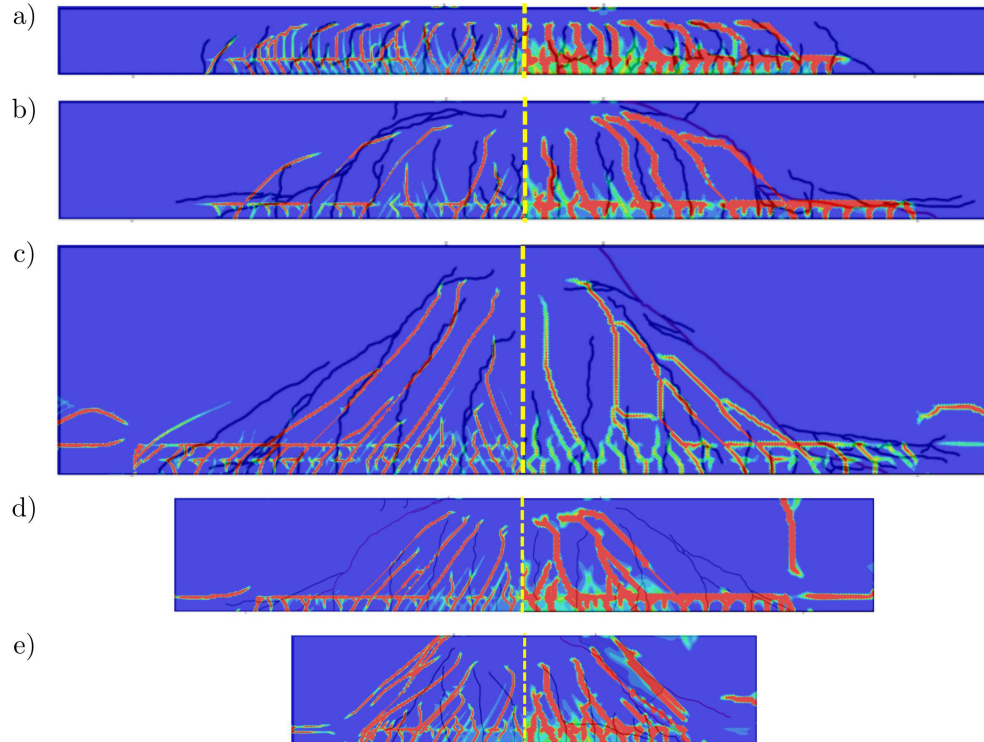
FIG. 14. Smeared crack patterns obtained with the concrete damaged plasticity model with
dense (left hand side) and coarse (right hand side) mesh for beam: S1D18a108 (a),
S1D36a108 (b), S1D72a108 (c), S2D36a72 (d) and S2D36a36 (e).

with the isotropic damage model. However, the CDP model produced crack patterns affected by the FE mesh definition, while the coupled model (especially) and the elasto-plastic model gave more realistic maps.

These four constitutive laws share several components in their formulation and it is desirable to identify the most critical ones. This is the topic of ongoing research. The attention is focused on the analysis on the material point level to get a better understanding of the performance of each constitutive law in simulations of RC beams under mixed shear failure modes.

Acknowledgements

References

1. P. MENÉTREY, K.J. WILLAM, *Triaxial failure criterion for concrete and its generalization*, ACI Structural Journal, **92**, 3, 311–318, 1995.

2. P.H. FEENSTRA, R. DE BORST, *A composite plasticity model for concrete*, International Journal of Solids and Structures, **33**, 5, 707–730, 1996.

3. P. PIVONKA, J. OŽBOLT, R. LACKNER, H. MANG, *Comparative studies of 3D-constitutive models for concrete: application to mixed-mode fracture*, International Journal for Numerical Methods in Engineering, **60**, 2, 549–570, 2004.

4. J. MAZARS, *A description of micro- and macroscale damage of concrete structures*, Engineering Fracture Mechanics, **25**, 5-6, 729–737, 1986.

5. R.H.J. PEERLINGS, R. DE BORST, W.A.M. BREKELMANS, M.G.D. GEERS, *Gradient enhanced damage modelling of concrete fracture*, Mechanics of Cohesive-Frictional Materials, **3**, 323–342, 1998.

6. R. DE BORST, P. NAUTA, *Non-orthogonal cracks in a smeared finite element model*, Engineering Computations, **2**, 3, 35–46,1985.

7. R. DESMORAT, F. GATUINGT, F. RAGUENEAU, *Nonlocal anisotropic damage model and related computational aspects for quasi-brittle materials*, Engineering Fracture Mechanics, **74**, 10, 1539–1560, 2007.

8. J. PAMIN, R. DE BORST, *Stiffness degradation in gradient-dependent coupled damage-plasticity*, Archives of Mechanics, **51**, 3-4, 419–446, 1999.

9. G. MESCHKE, R. LACKNER, H.A. MANG, *An anisotropic elastoplastic-damage model for plain concrete*, International Journal for Numerical Methods in Engineering, **42**, 4, 702–727, 1998.

10. P. GRASSL, D. XENOS, U. NYSTROM, R. REMPLING, K. GYLLTOFT, *CDPM2: a damage-plasticity approach to modelling the failure of concrete*, International Journal of Solids and Structures, **50**, 3805–3816, 2013.

11. R. DE BORST, L.J. SLUYS, *Localisation in a Cosserat continuum under static and dynamic loading conditions*, Computer Methods in Applied Mechanics and Engineering, **90**, 1-3, 805–827, 1991.

12. J. TEJCHMAN, E. BAUER, *Numerical simulation of shear band formation with a polar hypoplastic constitutive model*, Computers and Geotechnics, **19**, 3, 221–244, 1996.

13. G. PIJAUDIER-CABOT, Z.P. BAŽANT, *Nonlocal damage theory*, Journal of Engineering Mechanics ASCE, **113**, 10, 1512–1533, 1987.

14. Z.P. BAŽANT, M. JIRÁSEK, *Nonlocal integral formulations of plasticity and damage: survey of progress*, ASCE Journal of Engineering Mechanics, **128**, 11, 1119–1149, 2002.

15. J. PAMIN, *Gradient-dependent Plasticity in Numerical Simulations of Localization Phenomena*, PhD Thesis, Delft University of Technology, 1994.

16. W.M. WANG, L.J. SLUYS, R. DE BORST, *Viscoplasticity for instabilities due to strain softening and strain-rate softening*, International Journal for Numerical Methods in Engineering, **40**, 20, 3839–3864, 1997.

17. M. Ortiz, A. Pandolfi, *Finite-deformation irreversible cohesive elements for three-dimensional crack propagation analysis*, International Journal for Numerical Methods in Engineering, **44**, 9, 1267–1282, 1999.

18. F. Zhou, J.F. Molinari, *Dynamic crack propagation with cohesive elements: a methodology to address mesh dependency*, International Journal for Numerical Methods in Engineering, **59**, 1, 1–24, 2004.

19. G.N. Welss, L.J. Sluys, *A new method for modelling cohesive cracks using finite elements*, International Journal for Numerical Methods in Engineering, **50**, 12, 2667–2682, 2001.

20. N. Moes, T. Belytschko, *Extended finite element method for cohesive crack growth*, Engineering Fracture Mechanics, **69**, 7, 813–833, 2002.

21. K. Dörr, *Ein Bertrag zur Berechnung von Stahlbetonscheiben unter besonderer Berücksichtigung des Verbundverhaltens*, Dissertation, Darmstadt Universität, 1980.

22. J.V. Cox, L.R. Herrmann, *Development of a plasticity bond model for steel reinforcement*, Mechanics of Cohesive-Frictional Materials, **3**, 2, 155–180, 1998.

23. T. Małecki, I. Marzec, J. Bobiński, J. Tejchman, *Effect of a characteristic length on crack spacing in a reinforced concrete bar under tension*, Mechanics Research Communications, **34**, 5-6, 460–465, 2007.

24. A. Wosatko, J. Pamin, M.A Polak, *Application of damage–plasticity models in finite element analysis of punching shear*, Computers & Structures, **151**, 73–85, 2015.

25. D. Xenos, P. Grassl, *Modelling the failure of reinforced concrete with nonlocal and crack band approaches using the damage-plasticity model CDPM2*, Finite Elements in Analysis and Design, **117-118**, 11–20, 2016.

26. J. Oliver, D.L. Linero, A.E. Huespe, O.L. Manzoli, *Two-dimensional modeling of material failure in reinforced concrete by means of a continuum strong discontinuity approach*, Computer Methods in Applied Mechanics and Engineering, **197**, 5, 332–348, 2008.

27. J. Suchorzewski, E. Korol, J. Tejchman, Z. Mróz, *Experimental study of shear strength and failure mechanisms in RC beams scaled along height or length*, Engineering Structures, **157**, 203–233, 2018.

28. L. Pereira, J. Weerheijm, L.A. Sluys, *A numerical study on crack branching in quasi-brittle materials with a new effective rate-dependent nonlocal damage model*, Engineering Fracture Mechanics, **182**, 689–707, 2017.

29. L. Pereira, J. Weerheijm, L.A. Sluys, *Simulation of compaction and crushing of concrete in ballistic impact with a new damage model*, International Journal of Impact Engineering, **111**, 208–221, 2018.

30. J. Lee, G.L. Fenves, *Plastic-damage model for cyclic loading of concrete structures*, Journal of Engineering Mechanics ASCE, **124**, 8, 892–900, 1998.

31. J. Mazars, F. Hamon., S. Grange, *A model to forecast the response of concrete under severe loadings the μ damage model*, Procedia Materials Science, **3**, 979–984, 2014.

32. J. Mazars, F. Hamon., S. Grange, *A new 3d damage model for concrete under monotonic, cyclic and dynamic load*, Materials and Structures, **48**, 3779–3793, 2015.

33. P.E. Petersson, *Crack growth and formation of fracture zones in plain concrete and similar materials*, Report TVBM-3005, Division of Building Materials, Lund University of Technology, 1981.

34. D.A. Hordijk, *Local Approach to Fatigue of Concrete*, Ph.D. Thesis, Delft University of Technology, Delft, 1991.

35. J. Bobiński, J. Tejchman, *A coupled constitutive model for fracture in plain concrete based on continuum theory with non-local softening and eXtended Finite Element Method*, Finite Elements in Analysis and Design, **114**, 1–21, 2016.

36. J. Bobiński, J. Tejchman, *Comparison of continuous and discontinuous constitutive models to simulate concrete behaviour under mixed-mode failure conditions*, International Journal for Numerical and Analytical Methods in Geomechanics, **40**, 3, 406–435, 2016.

37. I. Marzec, J. Tejchman, *Computational modelling of concrete behaviour under static and dynamic conditions*, Bulletin of the Polish Academy of Sciences-Technical Sciences, **61**, 1, 85–95, 2013.

38. Ł. Skarżyński, I. Marzec, J. Tejchman, Experiments and numerical analyses for composite RC-EPS slabs, Computers and Concrete, **20**, 6, 689–704, 2017.

39. I. Marzec, J. Tejchman, Z. Mróz, *Numerical analysis of size effect in RC beams scaled along height or length using elasto-plastic-damage model enhanced by non-local softening*, Finite Elements in Analysis and Design, **157**, 1–20, 2019.

40. M.G.D. Geers, *Experimental Analysis and Computational Modeling of Damage and Fracture*, PhD Thesis, Eindhoven University of Technology, 1997.

41. Abaqus Documentation. Dassault Systemes, 2016.

42. J. Lubliner, J. Oliver, S. Oller, E. Onate, *A plastic-damage model for concrete*, International Journal of Solids and Structures, **25**, 3, 229–326, 1989.

43. R.B.J. Brinkgreve, *Geomaterial Models and Numerical Analysis of Softening*, PhD Thesis, Delft University of Technology, 1994.

44. Z. Bazant, B. Oh, Byung, *Crack band theory for fracture of concrete*, Matériaux et Constructions, **16**, 155–177, 1983.

45. I. Marzec, J. Tejchman, A. Winnicki, *Computational simulations of concrete behaviour under dynamic conditions using elasto-visco-plastic model with non-local softening*, Computers and Concrete. **15**, 4, 515–545, 2015.